Molecular Hydrogen Storage in Fullerenes – A Dispersion-Corrected Density Functional Theory Study

D. J. Durbin[†§], N. L. Allan[§], C. Malardier-Jugroot[†]

[†]Department of Chemistry and Chemical Engineering, Royal Military College of Canada, Kingston, Ontario K7K 7B4, Cecile.Malardier-Jugroot@rmc.ca

[§]School of Chemistry, University of Bristol, Bristol BS8 1TS, United Kingdom

Abstract

H_2 physisorption within curved carbon nanomaterials for potential fuel storage on board vehicles is studied using dispersion-corrected Density Functional Theory. Full C_n (n = 20, 60, 180, 540, 960) fullerenes were considered along with single-walled carbon nanotubes ((3,3), (5,5), (9,9)) and graphene to investigate the effects of curvature, confinement, platinum and non-metal (B, N, O) dopants, $C_{fullerene}$–H_2 and H_2–H_2 distances, H_2 orientation on $C_{fullerene}$–H_2 interactions. The study mainly focuses on H_2 stored within the fullerene with some investigation into external H_2. A significant attractive $C_{fullerene}$–H_2 interaction energy of -28 kJ/mol is observed for H_2 in curved carbon nanomaterials where H_2 molecules are located ca. 2.9 Å from carbon atoms in a highly confined system. Dopants have the potential to increase the favourability of $C_{fullerene}$–H_2 interactions when multiple H_2 molecules are present by affecting the orientation of H_2 molecules within the carbon nanomaterial. This paper presents analysis of several carbon nanosystems and then proposes possible materials for H_2 storage on board vehicles.

1. Introduction

The Earth's fossil fuel reserves are depleting quickly and their use creates significant environmental problems. Optimization of alternative fuels is key to sustainable energy usage. Hydrogen gas is a strong contender to replace gasoline in automobiles due to the increasing efficiency and uses of hydrogen fuel cells (FCs). Hydrogen FCs are preferred to combustion engines because they produce energy efficiently with minimal pollution through the combination of H_2 with O_2 to produce H_2O. Since their use in NASA's Gemini space program in the 1960's hydrogen FCs have entered the regular consumer market in a variety of automobiles. The most common fuel cells, PEMFCs (polymer electrolyte membrane FCs or proton exchange membrane FCs), use a proton exchange membrane to transfer the protons produced by H_2 splitting then combine with oxygen to form H_2O, and electrons, which are used to power the vehicle [1].

Hydrogen fuel cells have been extensively researched for the past six decades because hydrogen gas is a strong candidate to replace gasoline in automobiles. At 143.0 MJ/kg, H_2 has the highest energy density of common fuels by weight (ca. three times larger than gasoline). Unfortunately, it will not be commercially viable until reliable storage methods are developed. Storage of hydrogen is challenging because, at 0.0108 MJ/L, gaseous H_2 has the lowest energy density by volume (over 3000 times smaller than gasoline) and it is highly diffuse and buoyant [1]. Therefore, compact and efficient storage techniques must be developed.

Traditionally, hydrogen storage techniques are evaluated by analysis of the gravimentric density (GD) and volumetric density (VD) of the storage system. The GD is the weight percentage of hydrogen relative to the total weight of the system (hydrogen + storage medium). The VD is the mass of hydrogen stored per unit volume of the system. The US Department of Energy (DoE) has released 2015, 2017 and ultimate targets for H_2 storage. These targets address GD, VD and the ideal temperatures for H_2 sorption and release [2]. The DoE GD and temperature targets are shown in figure 1 along with the placement of current H_2 storage methods.

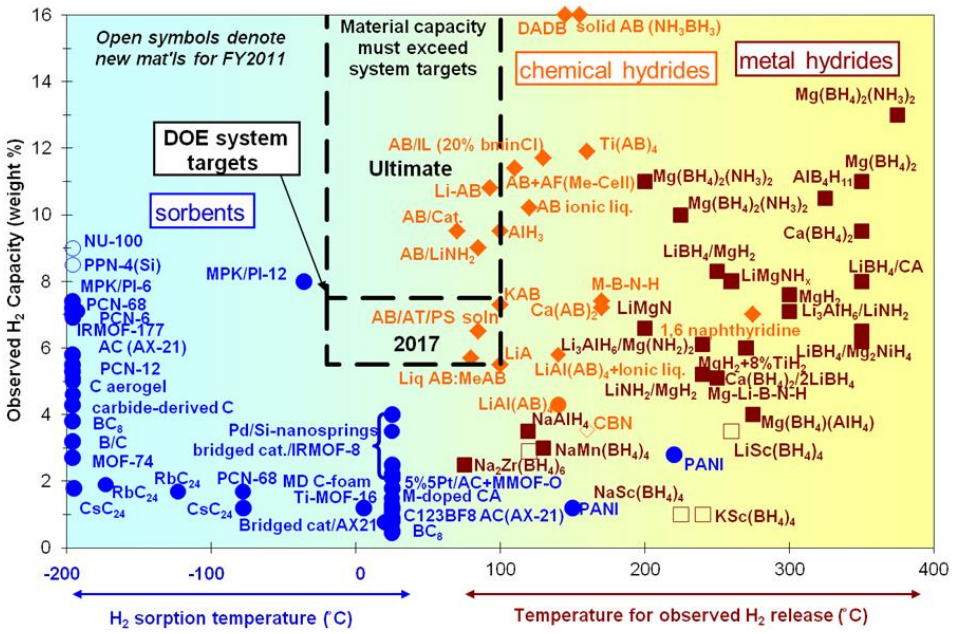

Figure 1 – US Department of Energy targets for gravimetric capacities and temperatures for H_2 sorption and release (2017 and ultimate) shown beside abilities of current storage methods. Reprinted with permission from S. Satyapal, US Department of Energy.

As shown in figure 1, at present the ammonia borane (AB) family of chemical hydrides are the only hydrogen storage methods that meet the DoE targets. However, these materials present challenges because the hydrogen is stored through the formation of chemical bonds so on board chemical reactions are required to release H_2. This can be done through thermal dehydrogenation when AB is in the solid state or solvolysis (hydrolysis or methanolysis) when in solution. Thermal dehydrogenation typically requires high temperatures and a large energy input. Therefore, AB hydrides can only be used if catalysts are added to assist in dehydrogenation. However, the use of catalysts produces problems of cost, deactivation and control of reaction kinetics [3]. Therefore, alternative storage methods are still under investigation.

The ideal storage media should be lightweight (to meet the GD requirements), inexpensive, and store a high density of H_2 by physisorption (to meet VD goals and limit the energy required to released H_2). Carbon nanostructures are a potential cheap, abundant, and lightweight storage system that has become increasingly prominent in the last few decades. Initial work began with carbon nanotubes (CNTs) in the late 1990s and has since expanded to include a wide variety of sp^2-hybridized carbon structures including graphene and spherical fullerenes [4-8]. Fullerenes have a theoretical maximum storage capacity of 58 hydrogen atoms in C_{60} (7.5 wt%) at 0 K. This

produces a metastable structure with an internal pressure of 1.3 Mbar. The practical storage capacity will be lower, but storage in fullerenes is still promising [9].

There are two main approaches to hydrogen storage on large area carbon nanomaterials. The first, hydrogen chemisorption, considers hydrogen chemisorbed on an expansive carbon surface to create C–H terminations through covalent bonds. The most extreme possibility is graphane, an extended 2-dimension hydrocarbon derived from chemisorption of hydrogen at every available position on graphene, leading to a GD of 8.3 wt%. Unfortunately, thermal annealing, a complex and high-energy processes, is required to add and remove hydrogen from this system so it is not commercially viable [10-12]. In general, hydrogen storage by chemisorption experiences the same issues observed with ammonia boranes with difficult and energetically expensive processes required to release H_2 on board a vehicle. In particular, both adsorption and desorption of hydrogen on carbon nanomaterials have energetic barriers greater than 100 kJ/mol [13].

The other method of hydrogen storage on carbon nanomaterials is via physisorption, in which H_2 is weakly attracted to the carbon surface by van der Waals forces. The strength of C–H_2 physisorption interactions is two orders of magnitude smaller than C–H chemisorption (368 – 535 kJ/mol) [14]. However, despite the lower interaction strength and volumetric storage density, physisorption is advantageous because it utilizes the benefits of carbon nanomaterials without requiring on board chemical reactions to release H_2 [15-16]. Therefore, physisorption is the method analyzed in the present study. A summary of the potential storage capacities of several carbon nanomaterials are illustrated in figure 2 relative to the DoE 2015 and ultimate targets.

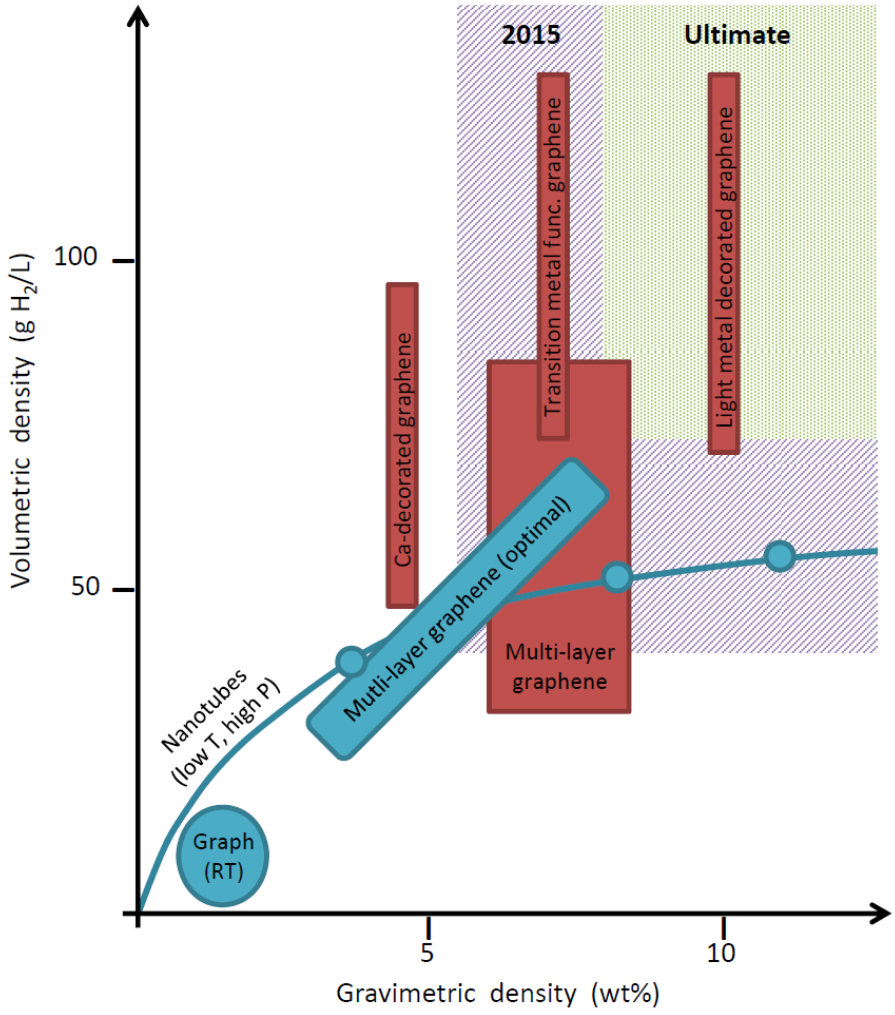

Figure 2 – Calculated and predicated H_2 storage capacity of several carbon sp^2-hybridized nanomaterials relative to the DoE 2015 and ultimate targets (purple and green boxes respectively). Chemisorption materials are shown in red; physisorption materials in blue. For chemisorption storage materials, a volumetric density range is estimated for a full system from single layer experiments. For physisorption on nanotubes, the points correspond to different nanotube sizes. Data from [13].

As can be seen in figure 2, carbon nanomaterials are promising for H_2 storage even though physisorption storage has lower VD's than chemisorption. This occurs because dispersion forces between carbon and hydrogen are weak, typically being less than 6 kJ/mol [17]. As a result, carbon substrates are often activated by introducing areas of sp^3-hybridized carbon or decorating with alkali or transition metals with care taken to avoid introducing chemisorption and additional weight. These modifications allow the substrate to contribute more electron density to the C–H_2

interaction and so strengthen the van der Waals forces to increase the GD and VD of the systems [18-20].

Many computational studies have been performed to determine the most favourable carbon nanomaterial for H_2 physisorption storage. Classical Monte Carlo studies of large carbon systems have concluded that the gravimetric storage capacity on flat carbon surfaces is greater than that on curved carbon. In addition, these studies also found that a larger GD can be obtained when there is a larger interlayer distance or diameter in graphite and carbon nanotubes respectfully. For instance, at 100 atm and 77 K, Rzepka et. al. reported a GD of 2.5 wt% in a SWCNT compared to 7 wt% in graphite when both systems have a C–C distance of 10.0 Å. At 100 atm and 77 K, Meregalli et. al. reported a GD of 12.5 wt% in graphite with a C–C interlayer of distance of 20 Å compared to 3 wt% in graphite with a C–C distance of 6 Å [13, 21-24].

Ab initio studies, in contrast, have found that hydrogen storage in curved carbon is more promising than in planar carbon substrates. These studies [25-27] have also concluded that an internal diameter near 6 Å is most favourable for C–H_2 interactions. For example, Chandrakumar et. al. found that the interaction energy of H_2 with a benzene ring increases from -7.0 kJ/mol on flat benzene to -9.8 kJ/mol on benzene with 35º of local curvature [27]. Patchkovskii predicted that a graphene interlayer distance of 6 Å is optimal for H_2 physisorption storage [17].

H_2 physisorption interactions are stronger on concave carbon surfaces because of the greater degree of sp^3-hybridization at areas of curvature. In addition, in curved surfaces different electron densities on the two sides of the surface are observed. On the convex side, electron density in the *p* orbitals is more available for chemisorption. On the concave side, the adjacent carbon atoms are closer, enhancing physisorption [13, 27, 28].

These *ab initio* studies have investigated optimization of H_2 storage on curved carbon nanomaterials by analyzing properties such as carbon bonding sites, orientation of H_2 and substrate curvature. They provide good preliminary understanding of H_2 physisorption on carbon nanomaterials with a high level of theory. However, analyses were performed on molecules containing only a very small number of carbon atoms, sometimes as little as five [27]. Therefore, these studies did not allow for the effects of multiple carbon interactions with one H_2 molecule, which can occur in large systems. Consideration of only a small surface section is also liable to spurious edge effects. To ensure that these effects are considered, the current study modeled complete fullerenes.

In order to produce the strongest H_2 physisorption storage with the smallest energy input, H_2 physisorption on carbon nanomaterials must be better understood. This is especially needed because previous Monte Carlo and *ab initio* studies produced conflicting results with Monte Carlo simulations finding flat carbon nanomaterials more favourable for H_2 storage and *ab initio* results finding curved materials more favourable. Therefore, the present study works to bridge the gap between classical Monte Carlo and *ab initio* simulations by analyzing large carbon systems with a high level of theory.

The present study uses DFT with dispersion corrections to model H_2 interactions with full C_n (n = 20, 60, 180, 540, 960) fullerenes. In order to analyze the effects of curvature and confinement, H_2 storage in the fullerenes is compared with single-walled carbon nanotubes of similar diameter and graphene. In addition, due to the higher H_2 storage capacities previously predicted and observed in carbon nanomaterials containing dopants (fig. 2), exohedral and substitutional platinum, and boron, nitrogen and oxygen substitutional dopants are considered in an attempt to strengthen the C–H_2 physisorption interaction.

Platinum was chosen because it has been shown to be useful for hydrogen storage, both as bulk platinum, due to strong Pt–H interactions [29], and for hydrogen spillover [30-31]. In addition, it is known that platinum nanoparticles disperse well on carbon nanomaterials, especially single-walled carbon nanotubes [32-33]. This has been confirmed by the authors in experimental studies (not shown here).

Boron, nitrogen, and oxygen substitutional dopants were chosen because these elements are similar in size to carbon and so substitute readily into the carbon material [34-35]. However, the differences between the dopant elements are such that they affect the electronic properties of the carbon nanomaterial differently and so could potentially affect hydrogen storage [36]. Boron and nitrogen dopants in carbon nanomaterials, both in the presence [37] and absence [38-39] of Pt, have been previously found to increase the rate of the oxygen reduction reaction, and thus prevent CO poisoning, in fuel cells. Oxygen dopants have not been extensively studied previously.

Platinum has been found to have strong interactions with carbon nanomaterials due to an exchange in electron density between the carbon and platinum valence electrons. Detailed studies also found that the platinum's core 4f electrons are involved, creating a very strong Pt–C interaction [40]. Further analyses found that nitrogen substitutional dopants affect the Pt–substrate interaction by drawing electron density from neighbouring carbon atoms to interact with Pt, in

addition to the N electron density. Boron dopants interact with the platinum valence *d* orbitals. Therefore, the presence of both N and B substitutional dopants increases the strength of the interaction between Pt and the carbon substrate [41].

This work extends previous studies on similar systems, which showed that modification of a graphene/Pt substrate can have a large effect on the interaction of the substrate with small gas molecules, including H_2 and CO [42-43].

2. Methods

All simulations were performed using Density Functional Theory (DFT) as implemented in the *Gaussian 09* software package [44]. The B3LYP functional was used to perform an initial analysis of H_2 interactions in all systems. B3LYP combines the Becke and Lee-Yang-Parr gradient correction energies with the exact non-local Hartree-Fock exchange energy to calculate the exchange-energy functional. This is particularly useful for systems containing transition metals because the functional is reliable for modeling the strong onsite Coulomb repulsions between *d* and *f* electrons including a substantial contribution from exact exchange [45-46]. An empirical dispersion correction was then added using the DFT-D3 software [47-48].

The LANL2MB basis set was used in conjunction with B3LYP because it is specifically designed for transition metals. Minimal and split-valence basis sets are very computationally expensive for atoms with a large number of electrons. LANL2MB, therefore, uses previously-determined effective potentials [49-51] to describe core electrons and a minimal basis set for valence electrons; in order minimize computation time, the STO-3G minimal basis set is used [52-53]. This combination allows some flexibility for the valence electrons while the frozen core potential does not significantly increase computation time. The B3LYP functional and the LANL2MB basis set have been shown to produce trustworthy results for similar systems [42-43].

More detailed analyses were performed on the most promising systems with the B97D functional. B97D includes dispersion interactions during optimization, which are very important when analyzing the interaction between H_2 and carbon. B97D is a generalized gradient approximation (GGA) type functional that combines Becke's power-series initial guess with

explicit parameterization including (damped) atom-pairwise dispersion corrections [54]. This functional has been shown to produce good results for similar systems [55]. Two basis sets were used for these calculations. The LANL2DZ basis set was employed for Pt; 6-311G(d,p) for C and H. LANL2DZ is similar to LANL2MB in that it uses a frozen core potential for large atoms but LANL2DZ uses D97V, a Dunning/Huzinaga valence double-zeta basis set, for the valence electrons [56]. The inclusion of polarization functions is often important for properties such as physisorption [57].

The results reported in sections 3.1.1, 3.1.4, 3.1.5, 3.1.6 were obtained with B3LYP/LANL2MB/DFT-D3 due to the size, complexity and large number of systems analyzed. All other results were obtained with B97D/LANL2DZ/6-311G(d,p). Results from both methods were compared for small systems and provided similar trends.

Calculations were carried out for complete fullerenes (C_n, n = 20, 60, 180, 540, 960) containing up to six internal H_2 molecules, one exohedral or substitutional Pt atom, and one to three substitutional non-metal dopant atoms (N, B or O) where applicable. One non-metal substitutional dopant was included in systems that also contained Pt, located directly under the Pt dopant; three non-metal substitutional dopants were used in systems without Pt, arranged in an alternating pattern within one six-membered ring. Similar systems containing a large carbon surface with a limited number of dopant atoms have been shown to be effective in previous studies by the authors, which investigated the interaction of carbon nanomaterials with H_2 and CO [42-43].

SWCNTs of the form (n,n) where n = 3, 5, 9 were modelled in a similar fashion. These nanotubes were chosen because they have similar diameters to C_{20}, C_{60} and C_{180} respectively and so are most useful for analyzing confinement effects. An 8.5 Å segment of nanotube was considered. Periodic boundary conditions were applied to the segment when the less computationally expensive B3LYP functional was used. The nanotube segment was hydrogen terminated when the B97D functional was applied. Graphene sheets were modelled with a hydrogen-terminated 14.5 x 14.8 Å section throughout.

Coordinates for the structures of the smaller fullerenes ($20 \leq n \leq 540$) were obtained from the *Computational Chemistry List, Ltd.* on-line fullerene database [58]. Coordinates for the C_{960} structure were provided by Henrard at the University of Namur. Coordinates for the SWCNTs

were generated by TubeGen On-line (version 3.4) [59]. All systems were optimized without constraints.

Once geomtries were optimized, the C–H_2 and H_2–H_2 bond distances and the fullerene–H_2 interaction energy, ΔE (eq. 1), were calculated. A negative value shows that the fullerene–H_2 systems is more stable than the sum of the carbon substrate and H_2 molecules individually.

$$\Delta E = E_{fullerene:nH_2} - \left[E_{fullerene:(n-1)H_2} + E_{H_2} \right] \qquad [1]$$

Basis set superposition error (BSSE) is always a concern when minimizing the energy of systems with multiple compounds as a function of geometry [60]. BSSE was considered in this study using the counterpoise correction method [61-63]. The correction ranged from ca. 9 kJ/mol for C_{20} systems to ca. 1 kJ/mol for C_{180}. It did not change any trends or conclusions.

Two computational methods were used in this study. Initially, a large number of systems were analyzed with B3LYP and LANL2MB with a DFT-D3 empirical dispersion correction. These allowed for characterization of the effects of fullerene size and curvature; H_2 confinement; nature, amount and location of dopants; and, optimal C–H_2 and H_2–H_2 distances. The most interesting systems were then further analyzed with B97D and LANL2DZ/6-311G(d,p).

The primary concern with B3LYP is that it does not include dispersion effects, which are the primary interaction in physisorption storage. However, the addition of the DFT-D3 correction does allow the characterization of dispersion effects. This was confirmed by comparison of systems run with both B3LYP/DFT-D3/LANL2MB and B97D/LANL2DZ/6-311G(d,p), which showed very similar results for C–H_2 interaction energy (differing by $\leq$3 kJ/mol for one H_2 molecule in C_n, $n \geq 60$). Identical trends in C–H_2 interactions were observed from both methods and so both methods are deemed satisfactory for the systems studied.

3. Results and Discussion

3.1. Effects on C–H_2 interaction energy with internal H_2

3.1.1. Curvature

When the position of H_2 within the fullerene is analyzed for C_n fullerenes of increasing diameter (n = 60, 180, 540, 960), an inverse correlation between fullerene size and C–H_2 interaction energy is observed (fig. 3). One hydrogen molecule in undoped C_{60} has an interaction energy of -27 kJ/mol. In the larger undoped C_{180} fullerene, this energy decreases to -4 kJ/mol and in the largest C_{540} and C_{960} fullerenes, the C–H_2 interaction is negligible, similar to that for graphene.

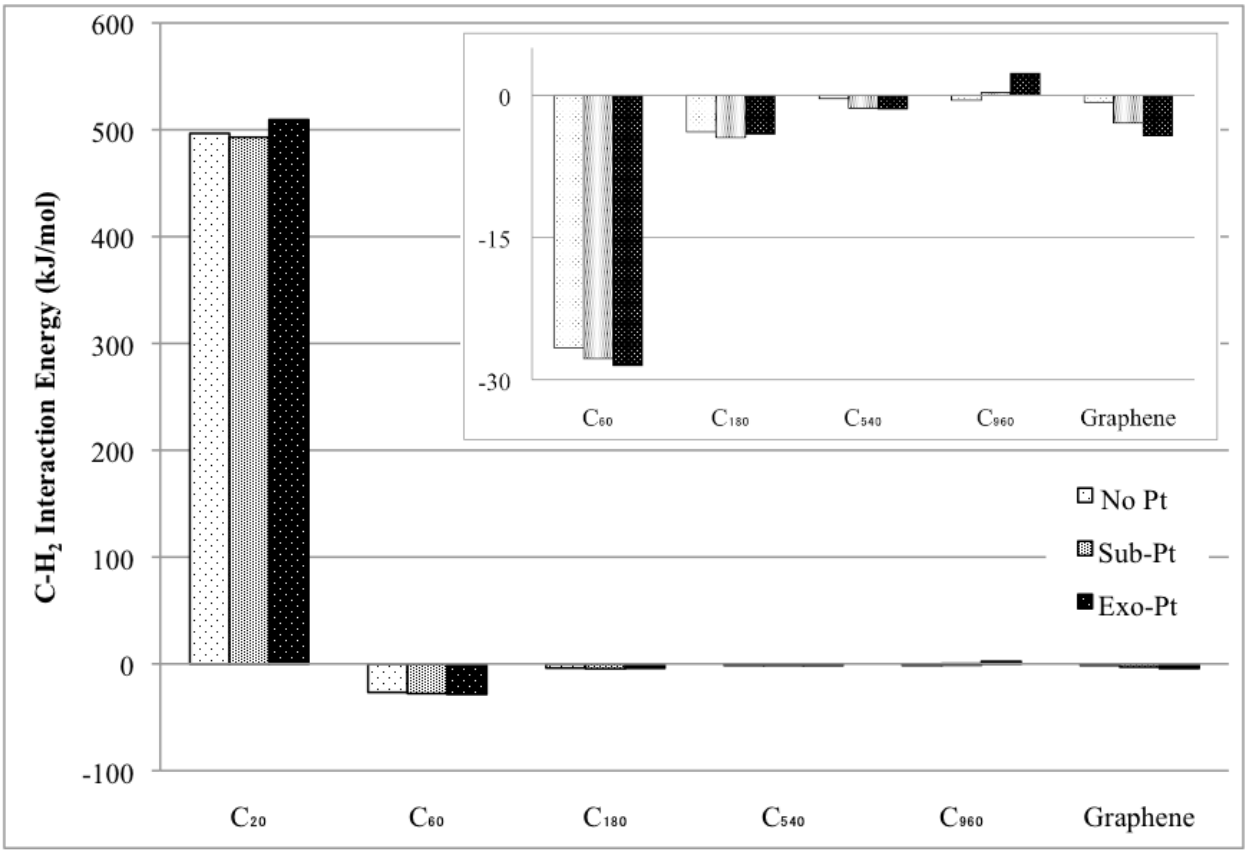

Figure 3 – C–H_2 interaction energies (kJ/mol) for C_{20}, C_{60}, C_{180}, C_{540}, C_{960}, graphene (undoped or with substitutional or exohedral platinum dopants), calculated with the B3LYP functional and LANL2MB basis set with a DFT-D3 dispersion correction. Insert shows magnification of C_{60}, C_{180}, C_{540}, C_{960}, graphene systems.

One of the primary reasons that the magnitude of C–H_2 interaction energy decreases with increasing fullerene size is the decreasing curvature. The transition of fullerene shape from a sphere at C_{60} to a polygon with flat sides at C_{960} is apparent in figure 4. This reduction of curvature occurs in larger fullerenes to reduce strain on the C–C σ bonds [64]. It has a large impact on H_2 physisorption because the large curvature in C_{60} allows a large number of carbon atoms to interact with the H_2 molecule. However, as the fullerene size increases, this interaction is lost as the fullerene surface becomes flatter. As a result, H_2 has an attractive interaction with C_{60} but the C–H_2 interactions in C_{540} and C_{960} are negligible.

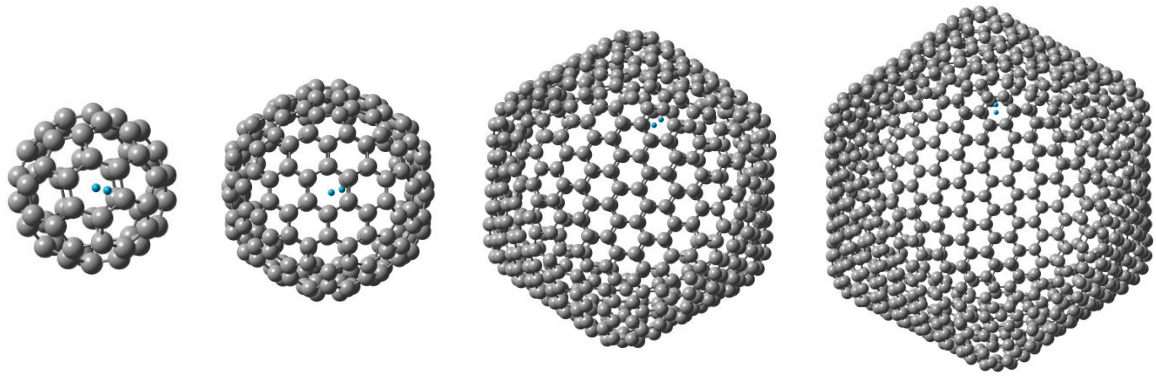

Figure 4 – Optimized geometry of C_{60}, C_{180}, C_{540} and C_{960} (containing internal H_2), calculated with B3LYP and LANL2MB (C = grey, H = light blue).

It should be noted that C_{20} is not considered in this section because of the large unfavourable C–H_2 interaction energy. This endothermic interaction is a result of heavy confinement of H_2 in the small fullerene that results in a small C–H_2 distance. This is discussed in section 3.1.2.

3.1.2. C–H_2 distance: One H_2 molecule

The characterization of the interaction energy as a function of the C–H_2 distance found that the shortest distance has a large influence on the magnitude of the C–H_2 physisorption interaction. Indeed, an optimal C–H_2 distance was observed at ca. 2.9 Å, the sum of the van der Waals radii of carbon and hydrogen [65]. When H_2 is forced into a fullerene where a minimum distance of 2.9 Å cannot be achieved, such as C_{20} (diameter = 3.7 Å), repulsive interactions dominate. This leads to a C–H_2 interaction energy of 509 kJ/mol, an unfavourable interaction, the magnitude of which is 20x larger than the favourable interaction observed in C_{60} (-25 kJ/mol).

In contrast, one H_2 molecule in C_{60} (diameter = 7.0 Å), where H_2 is ca. 2.9 Å from each carbon atom, experiences a notable attractive interaction. The C–H_2 interaction then decreases as H_2 moves more than 2.9 Å from the fullerene wall in larger systems (C_{180}, C_{540}, C_{960}). This was observed, for example, when the interaction energy of H_2 with C_{180} was calculated with the B97D functional without optimizing the position of H_2 within the fullerene. When H_2 is 4.9 Å from the fullerene wall, the C–H_2 interaction energy is -5.2 kJ/mol; when H_2 is 2.8 Å from the fullerene surface, the interaction energy is -12.8 kJ/mol occurs. This finding furthers those of Cabria et. al. and Patchkovskii et. al. who found that a C–H_2 distance of 2.7 Å, or a graphene interlayer separation of ca. 6 Å, is optimal for a (flat) layered graphite structure storing H_2 [17,66].

3.1.3. C–H_2 distance: Two H_2 molecule

When the C–H_2 interaction energy is calculated for the addition of a second H_2 molecule to a carbon system that already contains one H_2 molecule, the C–H_2 interaction is repulsive in C_{60} (fig. 5). This occurs because the small size of C_{60} forces the C–H_2 distance below 2.9 Å upon addition of multiple H_2 molecules. In contrast, at least six H_2 molecules (fig. 6) can be added to C_{180} without repulsive C–H_2 interactions because even with six hydrogen molecules in C_{180}, the C–H_2 distance does not decrease below 2.9 Å. This is discussed further in section 3.1.4.

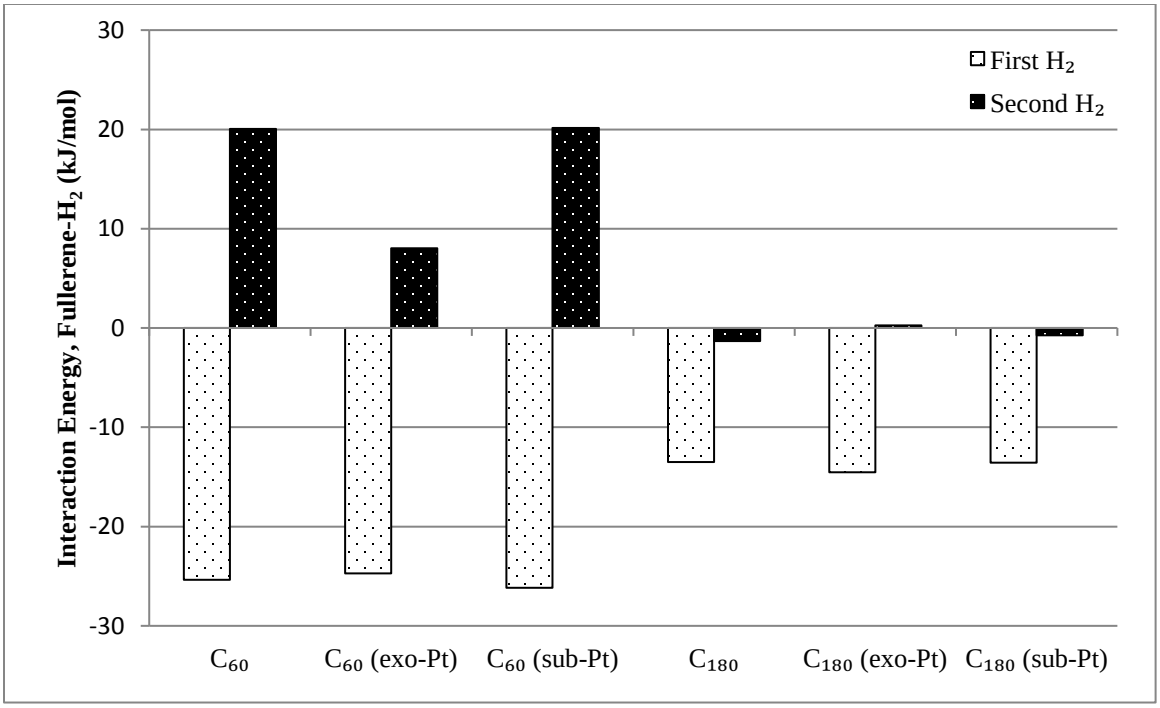

Figure 5 – Fullerene–H_2 interaction energies (kJ/mol) for C_{60} and C_{180} (undoped or with substitutional or exohedral platinum dopants) for addition of a first and then a second H_2 molecule, calculated with the B97D functional and 6-311G(d,p) (for C, H) and LANL2DZ (for Pt).

In larger systems, such as C_{180}, the C–H_2 interaction energy correlates strongly with the position of H_2 within the fullerene. For example, for two H_2 molecules in C_{180} there is a C–H_2 interaction energy of ca. -20 kJ/mol when the H_2 molecules are placed 2.7 Å from the fullerene wall. However, when there is a C–H_2 separation of 3.8 Å, the C–H_2 interaction decreases to ca. -8 kJ/mol.

3.1.4. C–H_2 distance: Multiple H_2 molecules

As seen in section 3.1.2, addition of subsequent H_2 molecules to a C_{60} system that already contains an H_2 molecule requires an input of energy. However, at least six H_2 molecules can be added to C_{180} exothermically (fig. 6).

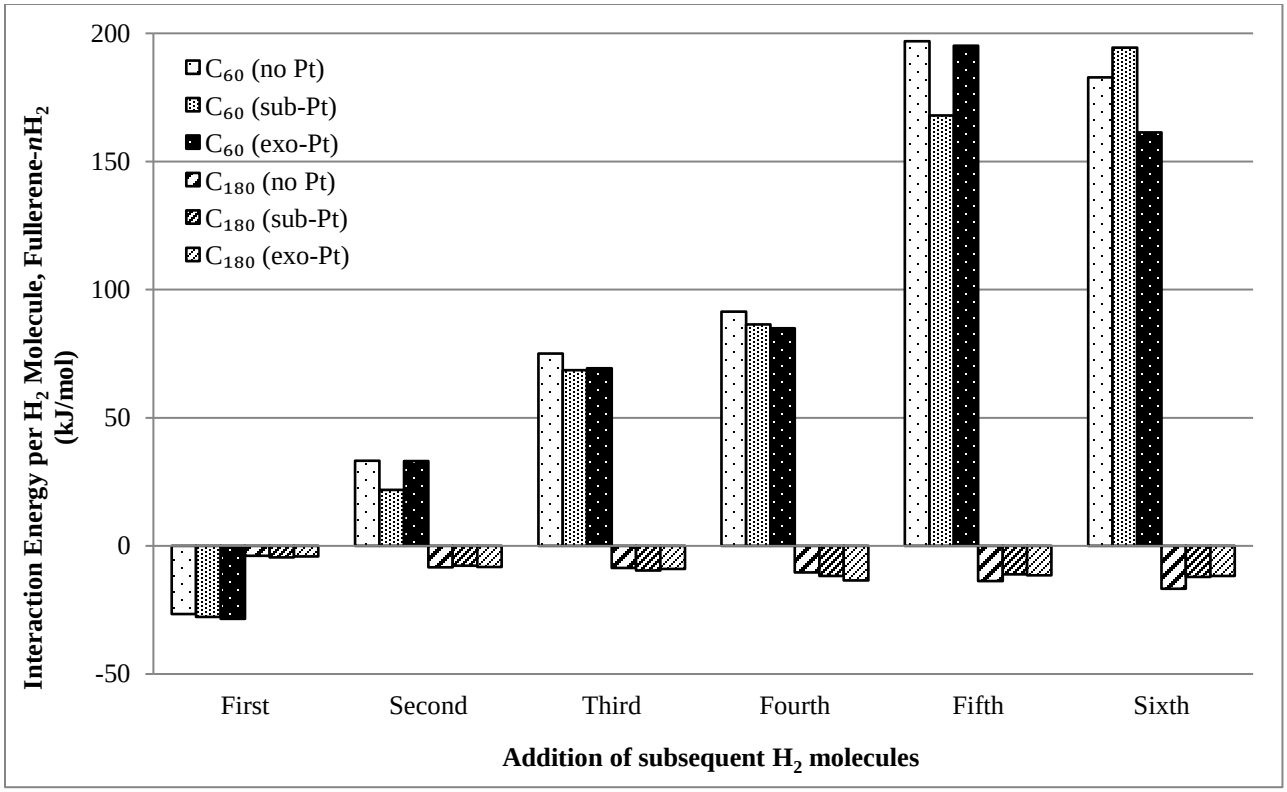

Figure 6 – Fullerene–nH_2 interaction energies per H_2 molecule (kJ/mol) for C_{60} and C_{180} (undoped or with substitutional or exohedral platinum dopants) for addition of successive H_2

molecules, calculated with the B3LYP functional and LANL2MB basis set with a DFT-D3 dispersion correction.

Figure 6 shows that addition of multiple H_2 molecules to C_{60} becomes increasingly endothermic for each subsequent H_2. Addition of a second H_2 molecule requires an input of 21–33 kJ/mol; 68–91 kJ/mol is then needed for addition of each of the third and fourth H_2 molecules; finally, 161–196 kJ/mol is necessary to add the fifth or the sixth.

As seen in section 3.1.3, an energy input is required to add the second H_2 molecule to C_{60} because the minimum C–H_2 distance decreases to as low as 2.5 Å. A greater energy input is then required for the third and fourth H_2 molecules because the C–H_2 distance decreases to as little as 2.2 Å. This C–H_2 distance does not change as the fifth and sixth H_2 molecules are added to C_{60} but more energy is required to add these later H_2 molecules. In order to accommodate them, the H_2–H_2 distance decreases to 1.5 Å, substantially smaller than the combined van der Waals radii of two hydrogen atoms (2.4 Å). As a result, the H_2 molecules experience repulsive interactions with other H_2 molecules as well as with the fullerene wall. In contrast to C_{60}, the H_2–H_2 distances in C_{180} never decrease below 2.2 Å and this system does not show any repulsive interactions.

The location of two, four, and six H_2 molecules in C_{60} is shown in figure 7. It can be seen that the H_2 molecules orient to produce a symmetrical configuration within the fullerene.

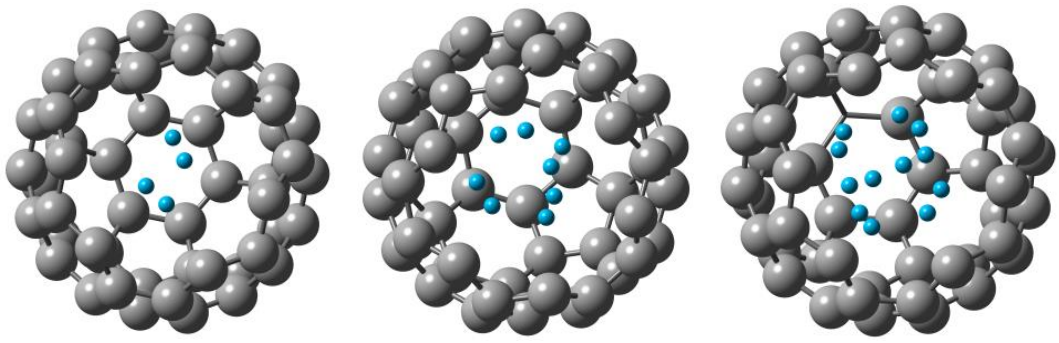

Figure 7 – C_{60} fullerenes optimized with two (left), four (middle) and six (right) internal H_2 molecules. The topmost six carbon atoms have been excluded to observe the H_2 molecules more clearly, calculated with B3LYP and LANL2MB (C = grey, H = light blue).

3.1.5. Platinum dopants

The results presented in section 3.1.1 also show the binding energies of H_2 in fullerenes doped with a substitutional or exohedral platinum atom (fig. 8). Figure 3 indicates that the binding

energies are similar with and without a metal dopant. The presence of a Pt dopant is insignificant to the C–H_2 interaction energy when one H_2 is contained within the fullerene. The interaction energies presented in figure 3 appear to differ slightly between undoped and doped fullerene system but these differences are negligible considering the uncertainty in the method. For example, in C_{60} the basis set superposition error is 3–4 kJ/mol, which is greater than the difference of 2 kJ/mol between the C–H_2 interaction energy for an H_2 molecule within an undoped and doped fullerene.

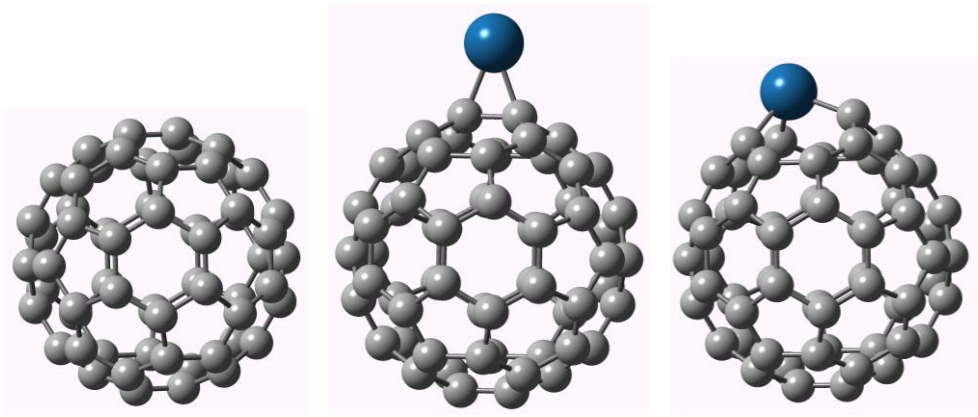

Figure 8 – Optimized geometry of undoped C_{60} (left) and C_{60} containing an exohedral Pt (middle) and substitutional Pt (right) dopant, calculated with B3LYP and LANL2MB (C = grey, Pt = dark blue).

The presence of exohedral Pt does not affect the C–H_2 interaction energy for internal H_2. However, substitutional Pt can affect the C–H_2 interaction energy. When the second and fifth H_2 molecules are added to C_{60} systems, the presence of substitutional Pt decreases the magnitude of the C–H_2 repulsive energy compared to undoped fullerenes or those with exohedal Pt (fig. 6). The substitutional Pt decreases the symmetry of the arrangement of H_2 molecules within the fullerene because the H_2 molecules become perpendicular to each other instead of parallel (fig. 9). The H_2–H_2 distance then increases slightly, which enhances favourability of the C–H_2 interaction because there is less H_2–H_2 repulsion. It should be noted that the average interaction energy is not substantially affected by the presence of Pt.

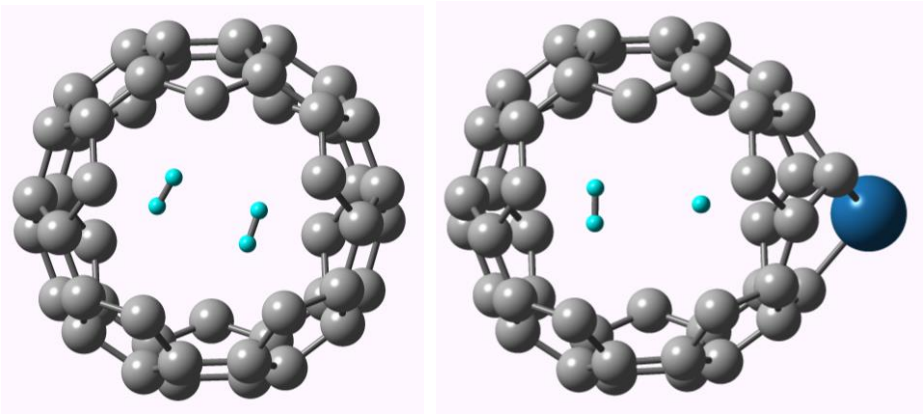

Figure 9 – Undoped C_{60} fullerene (left) and C_{60} with substitutional Pt (right) optimized with two internal H_2 molecules showing the change in orientation of the H_2 molecules caused by the presence of a substitutional Pt dopant. The bottom and topmost five carbon atoms have been excluded to observe the H_2 molecules more clearly, calculated with B3LYP and LANL2MB (C = grey, H = light blue, Pt = dark blue).

Exohedral Pt dopants were not observed to affect the C–H_2 interaction energy or H_2 geometry. It is well known that metallic Pt (or Pt at the surface) forms a strong bond with H_2 via chemisorption, which breaks the H–H bond to form two Pt–H bonds [67]. However, this is not possible here because of the barrier between H_2 and Pt created by the carbon surface. This suggests that the potential for Pt–H_2 chemisorption interactions is insufficient to cause a geometric change that would enable H_2 to be in closer physical contact with sub-Pt or exo-Pt in fullerenes. As result, only Pt–H_2 physisorption interactions are present in these systems.

Analysis of the natural bond orbitals (NBOs) of undoped and Pt-doped C_{60} finds that the addition of both substitutional and exohedral platinum dopants affects the electron density within the fullerene with sub-Pt having a larger effect. The change in NBO occupancy was calculated from equation 2, which compares the electron density of a Pt/fullerene–H_2 system to the Pt/fullerene and H_2 individually. A positive value indicates that the orbital gains electron density in the Pt/fullerene–H_2 system compared to the Pt/fullerene and H_2 separately, suggesting that this orbital is involved in a Pt/fullerene–H_2 (C–H_2 or Pt–H_2) interaction.

$$\Delta NBO = NBO_{Pt/fullerene:H_2} - \left[NBO_{Pt/fullerene} + NBO_{H_2}\right] \quad [2]$$

All these NBO analyses were calculated with B3LYP and LANL2MB. The C_{60} systems were also analyzed with B97D and LANL2DZ/6-311G(d,p). The results from both methods

showed identical trends. However, the changes in electron density were found to be larger with B97D, which models dispersion interactions more accurately.

As shown in figure 10, electron density becomes localized on Pt and a small number of carbon atoms when a platinum dopant is present. This suggests that the H_2 molecule interacts primarily with these atoms.

In particular, H_2 is found to interact with the Pt atom and one carbon atom on the opposite side of the Pt/fullerene. When platinum is substituted into the fullerene, H_2 interacts with all the valence orbitals of the Pt atom and does not interact with the carbon atoms surrounding the Pt dopant. When Pt is an exohedral dopant on the fullerene, H_2 does not have direct access to the Pt atom and so it interacts only with the platinum $5p_x$ orbital and also interacts with the carbon atoms neighbouring the Pt dopant.

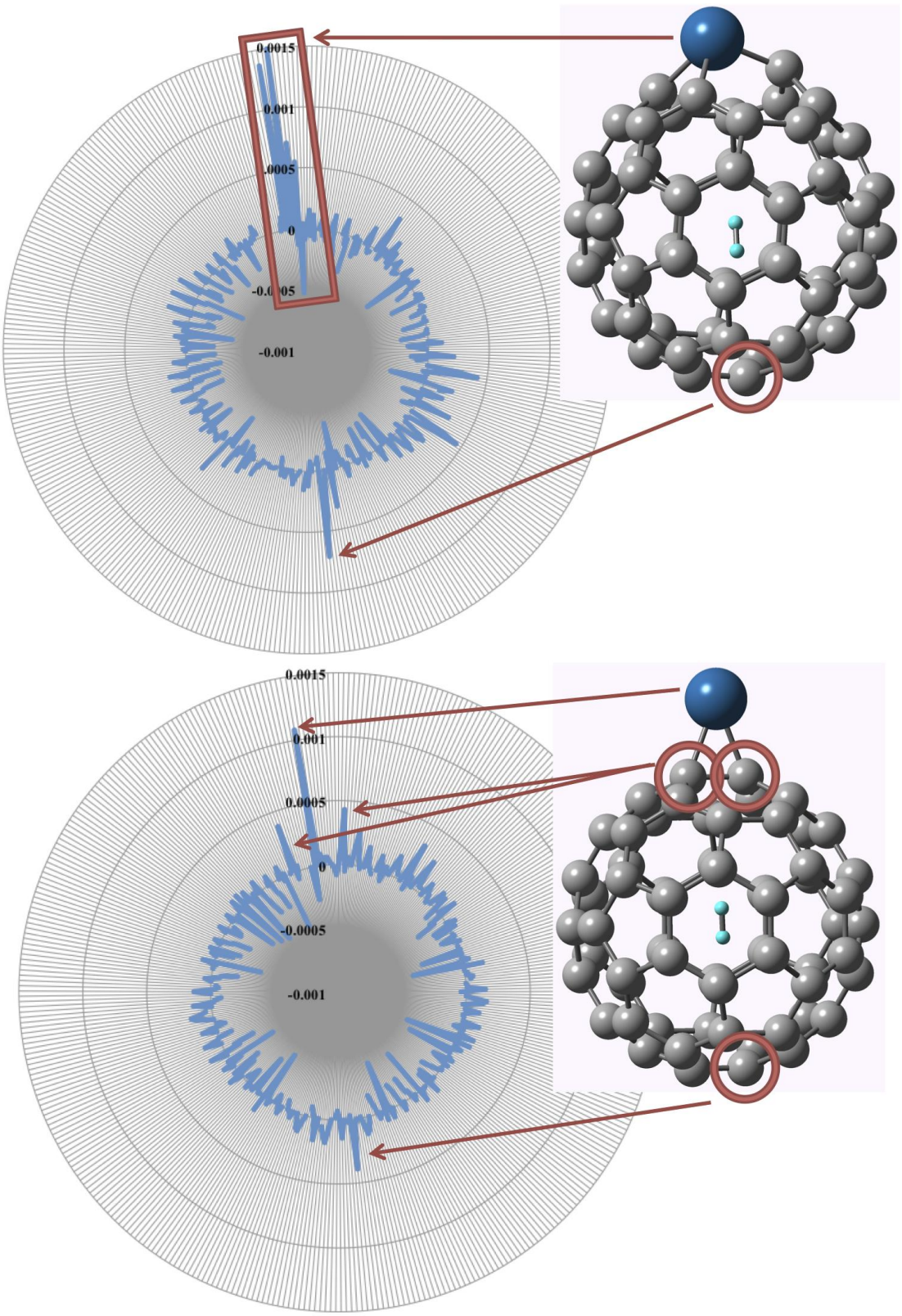

Figure 10 – Difference in natural bond orbital electron density of C and Pt orbitals in a Pt/fullerene containing H_2 compared to an empty Pt/fullerene for C_{60} with substitutional Pt (top)

or exohedral Pt (bottom). All C and Pt valence orbitals (*s*, *p*, *d*) are shown. A positive value indicates that the orbital gains electron density when H_2 is located in the Pt/fullerene, calculated with B3LYP and LANL2MB (C = grey, H = light blue, Pt = dark blue).

The interaction of H_2 with atoms located at opposite ends of the Pt/fullerene is primarily observed when H_2 is stored in C_{60} and not the larger fullerenes because in C_{60}, H_2 is located in the centre of the Pt/fullerene (ca. 2.9 Å from all atoms) so it is possible for H_2 to experience a dispersion interaction with atoms on opposite sides of the cage. In contrast, in the larger fullerenes, H_2 is located to one side of the cage where it is only 2.9 Å from a smaller number of atoms and dispersion interactions fall off rapidly with distance.

In C_{20}, there is a large change in electron density at all the carbon atoms and platinum when H_2 is incorporated. This is in contrast to the larger fullerenes where the platinum orbitals show notably larger changes in electron density than the carbon orbitals. In C_{20} the H_2 interaction is strongly endothermic and there is a large repulsive interaction of H_2 with all the atoms in the cage.

Although not depicted in figure 10, a substantial change (>0.001) in the electron density of the hydrogen atoms between H_2 contained within the Pt/fullerene and individual H_2 is required for a strong Pt/fullerene–H_2 interaction. The change in electron density of the hydrogen atoms in H_2 is 10x larger in C_{20} than C_{60} and it is negligible in C_{180}.

There is also a fundamental change in the type of interaction between these fullerenes. In C_{20}, repulsive interactions dominate, making the process endothermic. However, in the larger fullerenes, the interaction is exothermic because dispersion determines the overall weak C–H_2 interaction.

3.1.6. Non-metal dopants

Non-metal dopants showed promising effects in previous work by two of the authors when investigating CO and H_2 binding to Pt/graphene systems [42-43]. Addition of non-metal substitutional dopants to the Pt-doped graphene surface changed the electron density in the Pt–C interaction, which in turn altered the Pt–gas interaction. In the present study, one or three boron (electron acceptor) or nitrogen or oxygen (electron donor) dopants replaced carbon atoms in C_{60} and C_{180} and the effect on the C–H_2 interaction was observed with and without Pt dopants. The boron-doped fullerenes are shown in figure 11.

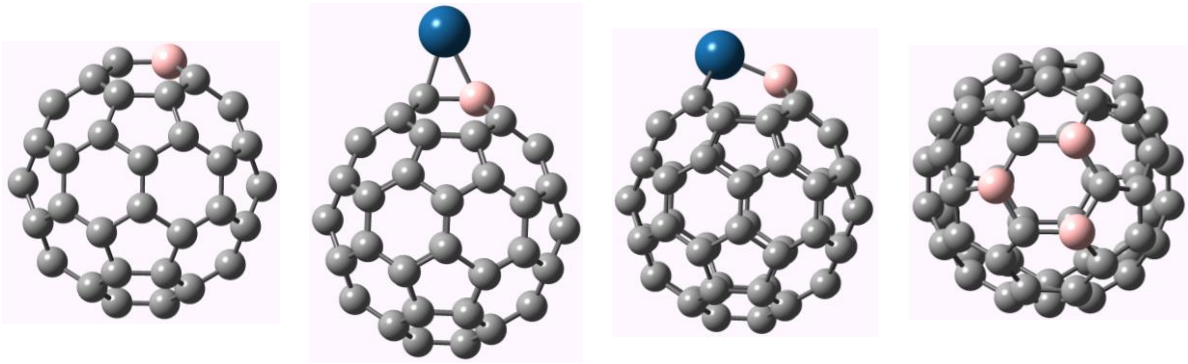

Figure 11 – Optimized geometry of B-doped C_{60} fullerenes (C = grey, Pt = blue, B = pink). Systems containing one boron atom where optimized with B3LYP and LANL2MB; the fullerene with three boron atoms was optimized with B97D and 6-311G(d,p).

In systems containing platinum, the non-metal dopant was substituted for one of the carbon atoms directly connected to the Pt atom. These systems were analyzed with B3LYP and LANL2MB with a DFT-D3 dispersion correction. Addition of a non-metal dopant does not affect the C–H_2 interaction energy (fig. 12). This is consistent with the polarizability of these dopants relative to carbon.

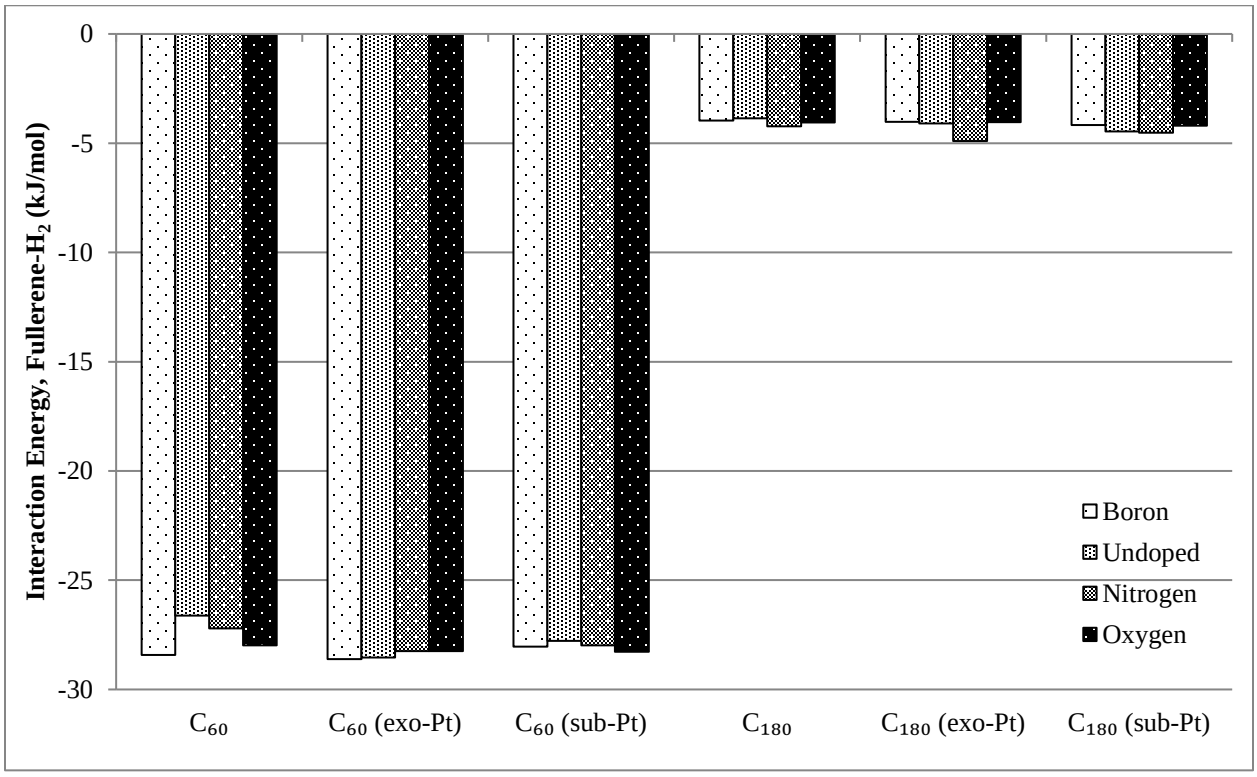

Figure 12 – Fullerene–H_2 interaction energies (kJ/mol) for C_{60} and C_{180} (undoped or with substitutional or exohedral platinum dopants) for systems containing no non-metal dopants and those doped with boron, nitrogen or oxygen, calculated with the B3LYP functional and LANL2MB basis set with a DFT-D3 dispersion correction.

Substitution of three atoms in C_{60} with non-metal dopants was also studied. The dopant atoms were added in an alternating pattern to one of the benzene rings in the fullerene. These systems were then analyzed with B97D and LANL2DZ/6-311G(d,p). Even with this higher number of dopant atoms, the C–H_2 physisorption interaction was unaffected.

3.1.7. 2D and 3D Confinement

To further understand H_2 storage in curved carbon nanomaterials, the effects of 2-dimensional versus 3-dimensional confinement were studied by comparing fullerenes with (*m*,*m*) single walled carbon nanotubes (SWCNTs) of similar diameters. C_{20}, C_{60} and C_{180} fullerenes were compared with (3,3), (5,5) and (9,9) SWCNTs respectively.

As is shown in figure 13, identical trends in C–H_2 interaction energy are observed for the 2D and 3D systems. However, a difference is observed in the magnitude of the interaction energies for C_{20} versus SWCNT (3,3) and C_{60} versus (5,5). The interactions were endothermic and weakly exothermic respectively.

In both cases, there is a stronger C–H_2 interaction when confining H_2 in a 3D system, consistent with the larger number of both repulsive and attractive C–H_2 interactions. However, the C–H_2 interactions are similar in C_{180} and SWCNT (9,9). This shows that in systems with larger diameters, where there is minimal confinement in either system, the shape of the carbon structure does not significantly affect the magnitude of the C–H_2 interactions.

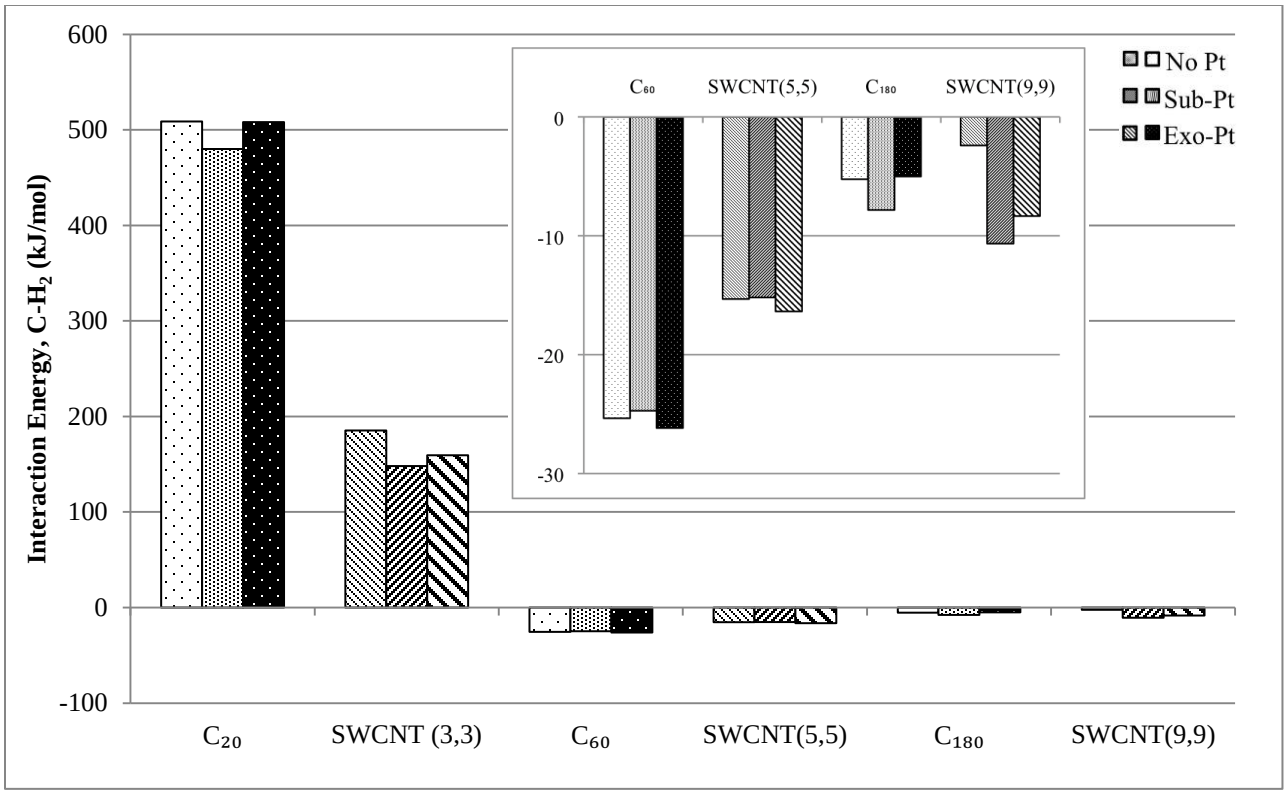

Figure 13 – C–H_2 interaction energies (kJ/mol) for H_2 inside C_{20}, C_{60} and C_{180} compared with (3,3), (5,5) and (9,9) SWCNTs respectively to determine the effects of 2D vs 3D confinement. Carbon systems are undoped or contain substitutional or exohedral platinum dopants. Insert shows a zoom in of C_{60}, C_{180}, SWCNT (5,5) and (9,9), calculated with the B97D functional and 6-311G(d,p) (for C, H) and LANL2DZ (for Pt).

Visualization of the molecular orbitals further indicated that the larger magnitude of C–H_2 interactions in the 3D system result from an increased number of C–H_2 interactions. As can be seen in figure 14, the H_2 $1\sigma_g$ orbital in C_{20} is spherical and can interact with every atom in the fullerene. In contrast, the H_2 $1\sigma_g$ orbital in SWCNT (3,3) is more angled and interacts only with the carbon atoms immediately surrounding the H_2 molecule.

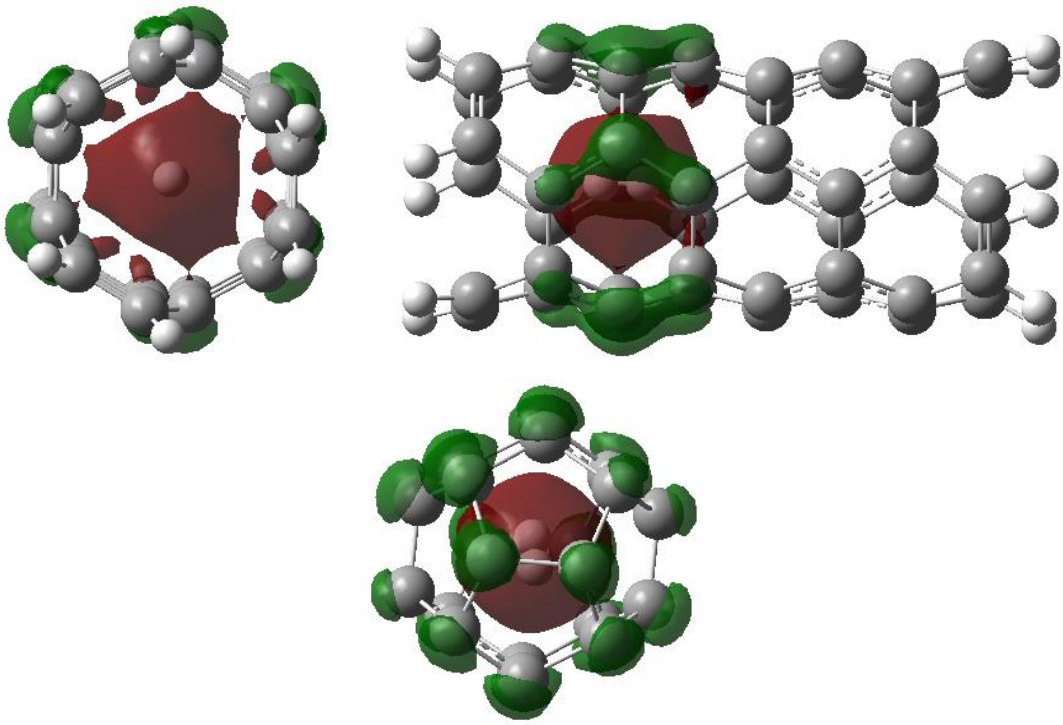

Figure 14 – Visualization of the H_2 $1\sigma_g$ molecular orbital in optimized SWCNT (3,3) (top) and C_{20} (bottom) systems showing the effect of confinement, calculated with B3LYP and 6-311G(d,p) (C = grey, H = white, H_2 molecular orbital = red/green). The orbitals displaced have an energy of -1387 kJ/mol for SWCNT (3,3) (orbital 92) and -1569 kJ/mol for C_{20} (orbital 37). All molecular orbitals were computed using an isovalue of 0.04.

The change in electron density of carbon and hydrogen orbitals between an individual carbon nanosystem and H_2 and H_2 confined within the carbon nanosystem is >10x greater in C_{60} compared to SWCNT (5,5). In addition, the changes in electron density in SWCNTs are localized on the carbon atoms surrounding the H_2 molecule; carbon atoms further along the nanotube are significantly less involved.

3.2 Effects on C–H_2 interaction energy with external H_2

This study has so far considered only the storage of H_2 within fullerenes on the concave surface. However, it is also important to understand how changes to the carbon structure affect H_2 that is external to the fullerene and so interacts with the convex surface. Ideally, H_2 will be stored both on the interior and the exterior surfaces of the fullerene to maximize efficiency of the storage system.

Figure 15 shows the C–H_2 interaction energy of C_n fullerenes (n = 20, 60, 180) with external H_2. The exothermic interaction of external H_2 in undoped systems is notable in C_{20} and then becomes negligible in the larger fullerenes. Similarly, the H_2 interaction with fullerenes containing substitutional Pt is larger in C_{20} and then decreases in C_{60} and C_{180}. In contrast, the interaction of H_2 with fullerenes containing exohedral Pt is weakest in C_{20} and then becomes stronger as the fullerene size increases.

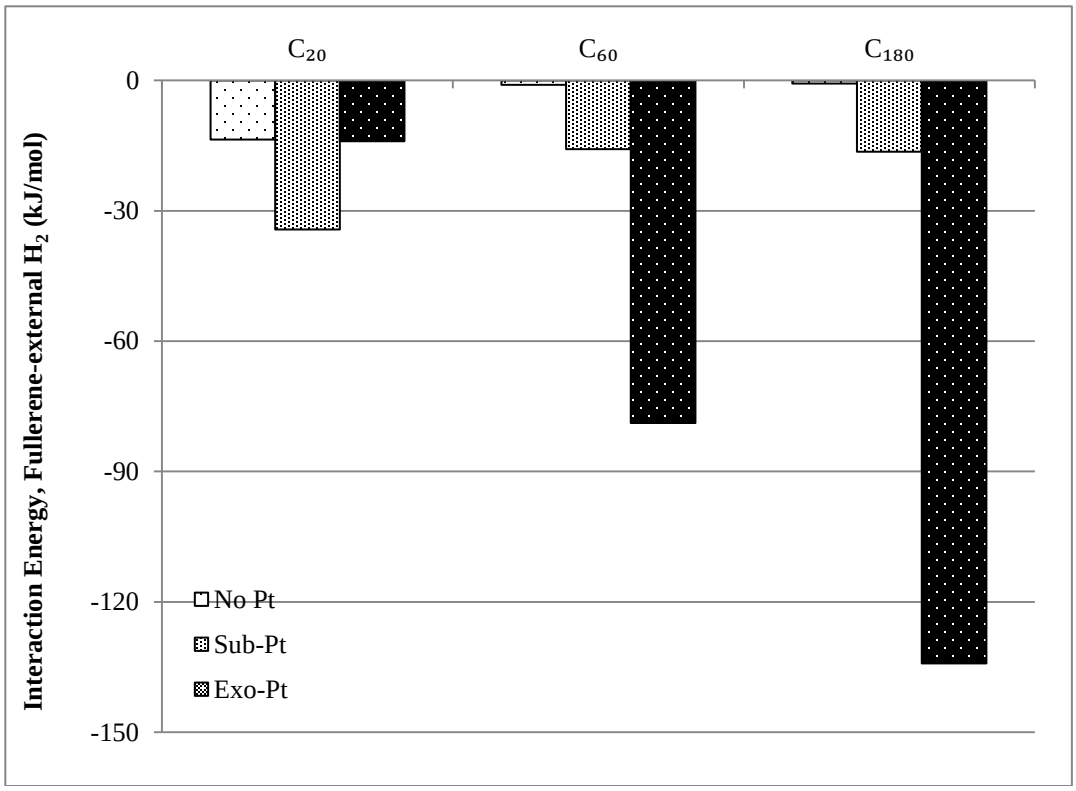

Figure 15 – Fullerene–H_2 interaction energies (kJ/mol) for C_{20}, C_{60} and C_{180} (undoped or with substitutional or exohedral platinum dopants) with external H_2, calculated with the B97D functional and 6-311G(d,p) (for C, H) and LANL2DZ (for Pt).

The interaction of external H_2 with undoped fullerenes suggests that there is only a notable C–H_2 interaction when the fullerene is very small (-14 kJ/mol in C_{20}). In the small fullerene, the curvature is so high that a large amount of electron density from the carbon *p* orbitals becomes available on the convex surface of the fullerene to interact with H_2, creating a physisorption interaction of -14 kJ/mol. Although previous research suggests that physisorption is favoured on a concave carbon surface [13], in the particular case of C_{20}, the convex surface shows a notable C–H_2 interaction, while H_2 cannot be placed within the fullerene to interact with the concave surface.

The notable C–H_2 interaction on the convex surface of C_{20} likely occurs because the high curvature of C_{20} produces greater sp^3 character in the carbon atoms.

In fullerenes containing substitutional Pt dopants, the C–H_2 interaction is strongest in C_{20} (-34 kJ/mol) and is then consistently weaker in C_{60} and C_{180} (-16 kJ/mol). It should be noted that Pt–H chemisorption bonds are not observed in the C_{60} and C_{180} systems because Pt is contained within the carbon surface and so does not have enough electron density available to bind with hydrogen due to a steric hindrance.

In contrast, the interaction of external H_2 with fullerenes containing exohedral Pt increases with fullerene size as the fullerene surface becomes flatter. When H_2 is placed external to a fullerene with exohedral Pt, there are no physical barriers between Pt and H_2 so H_2 dissociates and two Pt–H chemisorption bonds form. Previous studies by the research group found that the properties of an sp^2-hybridized carbon surface greatly influence the electron density in exohedral Pt that is available to interact with external molecules [42-43].

The interaction of external H_2 with SWCNTs was also investigated to determine the effect of the shape of the carbon material on its interactions with external H_2 (fig. 16). The trends are similar to those observed in figure 15 where the C–H_2 interaction is strongest in systems with exohedral Pt and weakest in undoped carbon nanomaterials. However, the C–H_2 interaction varies less between nanotubes of different diameters and is consistent with the absence of a clear flattening of the nanotube surfaces with increasing diameter, unlike the fullerenes (fig. 4).

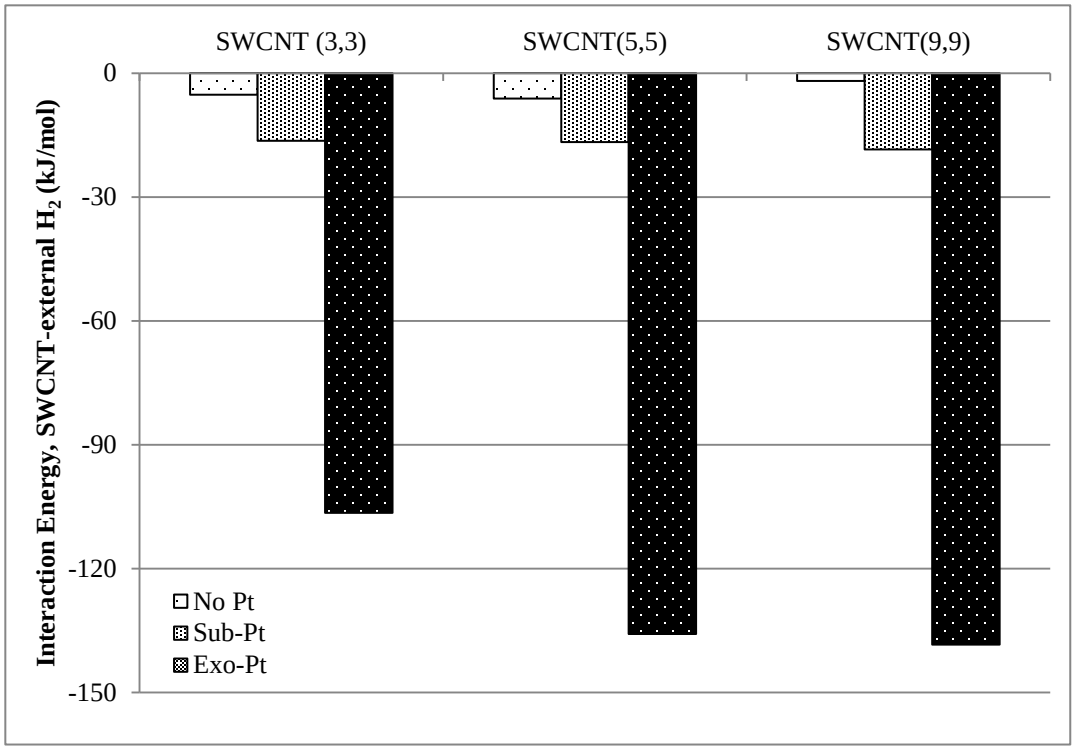

Figure 16 – SWCNT–H_2 interaction energies (kJ/mol) of (*n*,*n*) SWCNTs (*n* = 3, 5, 9) (undoped or with substitutional or exohedral platinum dopants) with external H_2, calculated with the B97D functional and 6-311G(d,p) (for C, H) and LANL2DZ (for Pt).

Finally, the interactions of external H_2 with fullerenes containing non-metal dopants were investigated with B3LYP and LANL2MB with a DFT-D3 correction. The trends observed in figure 15 were also observed for fullerenes containing non-metal dopants. However, in C_{180} with exohedral Pt, the presence of non-metal dopants decreases the Pt–H interaction significantly. This is consistent with previous studies by two of the authors [42-43], which found that the addition of non-metal dopants increase the strength of the Pt–C interaction. This effect appears to be more prominent in flatter systems.

3.3 Promising hydrogen storage systems

This study has investigated several properties of fullerenes with the overall objective of predicting a promising H_2 storage system for use on board vehicles. The storage system should be low cost, lightweight, straightforward to manufacture, and simple to use and refill. Carbon

nanomaterials are attractive for this purpose because they are relatively cheap, lightweight and abundant. Systems in which H_2 is physisorbed should allow for simple use and refilling.

H_2 was primarily modeled inside the fullerene because concave carbon surfaces are thought to be better for physisorption interactions [13]. The effect of curvature, confinement, Pt and non-metal (B, N, O) dopants to the fullerene, C–H_2 distances and the orientation of H_2 molecules were examined. The interaction of external H_2 was also briefly considered to provide further understanding of the systems. In conclusion:

(i) *Curvature:* Systems with higher curvature are more promising for H_2 physisorption because in more highly curved systems H_2 is able to interact with a greater number of carbon atoms.

(ii) *C–H_2 distance:* A C–H_2 distance of 2.9 Å is ideal for physisorption because this is the combined van der Waals radii of carbon and hydrogen. At this distance repulsive forces do not dominate, at larger distances the attractive dispersion interactions diminish.

(iii) *H_2 orientation:* When multiple H_2 molecules are within a fullerene, the molecules orient so that the distances of each H_2 molecule are equal from the fullerene surface. In addition, the most favourable interactions are observed when the H_2 molecules are at least 2.4 Å from each other. Dopants can affect the orientation of H_2 molecules and, consequently, the C–H_2 interaction energy.

(iv) *Platinum dopants:* The addition of substitutional or exohedral Pt dopants have a minimal effect on the C–H_2 interaction energy (and do not cause Pt–H chemisorption interactions) but addition of substitutional Pt can affect H_2 orientation within the fullerene.

(v) *Non-metal dopants:* Similar to Pt dopants, the addition of boron, nitrogen or oxygen non-metal dopants have minimal effect on the C–H_2 interaction energy. When non-metal and platinum dopants are combined, the effect of Pt is reduced.

(vi) *Confinement:* C–H_2 interactions have a large magnitude in highly confined systems because the H_2 molecule is able to interact with more carbon atoms. In general, this results in stronger C–H_2 interactions in smaller fullerenes and in fullerenes over

carbon nanotubes. However, it must be noted that in very highly confined systems, such as C_{20}, the C–H_2 interactions are repulsive; in large systems (C_{60} and larger), the C–H_2 interactions are attractive.

(vii) *External H_2:* The stronger interactions of external H_2 occur with systems containing exohedral Pt where the favourable fullerene–H_2 interaction increases with increasing fullerene size. H_2 shows a consistent weak attractive interaction with substitutional Pt in fullerenes of all sizes. H_2 typically has no external interaction with fullerenes that do not contain Pt dopants. An exception is C_{20}, which shows a notable exothermic interaction with external H_2 even without a Pt dopant. Single-walled carbon nanotubes of all sizes showed the same external H_2 interactions as the larger fullerenes. Non-metal dopants typically have little effect on C–H_2 interactions with external H_2 except that they reduce the interaction of H_2 with systems containing exohedral Pt.

From this study, two promising H_2 storage systems are proposed. One system involves H_2 storage within carbon nanotube/fullerene hybrides, such as those synthesized by Nasibulin et. al. (fig. 17) [70]. These structures, termed NanoBuds, are promising for H_2 storage because they can produce large carbon nanostructures containing spaces with a variety of curvatures and confinement. Once H_2 gas is inserted into these systems, the H_2 molecules can spread throughout the system, concentrating in areas of high curvature and confinement. Because of the size of the system, H_2 molecules will able to disperse adequately such that they will not be forced into positions where the C–H_2 distance or H_2–H_2 distance are less than 2.9 or 2.4 Å respectively.

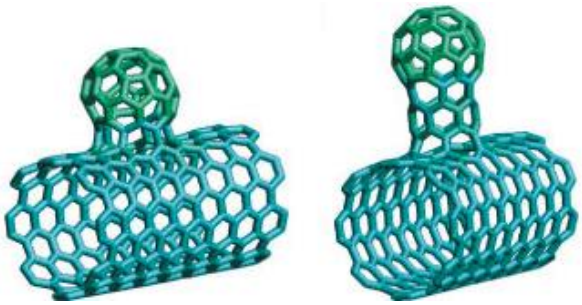

Figure 17 – Synthesized fullerene-SWCNT hybrid structures, termed NanoBuds. Reprinted from [70] with permission.

Another promising H_2 storage system will utilize the unexpectedly strong physisorption observed for H_2 external to C_{20}. It is well known that C_{60} fullerenes can form well-defined crystal structures [71-72]. Less research has gone into producing a crystal structure composed of C_{20} molecules. However, if C_{20} molecules were to form a crystal structure where the fullerene molecules are 5 – 6 Å apart, H_2 should be readily stored because of a large number of strong physisorption interactions.

Both of the proposed systems are open and so will not require extreme pressure to add or release H_2 from the system, such as would be required if H_2 was stored within a closed fullerene.

3.4 Exploratory storage systems: Heme dopants

Neither platinum or non-metal dopants are recommended because their effects on C–H_2 interactions are minimal and their inclusion would lead to higher production costs. Furthermore, addition of exohedral Pt could result in Pt–H chemisorption, which is undesirable for H_2 vehicle storage because complex on board endotherimc reactions would be required to release this hydrogen.

Nevertheless, because Pt dopants were found to influence the fullerene/H_2 electron density, more complex dopants should be considered for future storage systems. The present group has began research into a heme dopant, which is a heterogeneous dopant consisting of an iron atom surrounded by four nitrogen atoms inserted into a surface. When the heme dopant is combined with the desirable curvature and confinement properties of fullerenes, it is hoped that heme-fullerene systems will increase interaction with H_2 but sterically prevent chemisorption to the heme dopant, thereby producing a very favourable storage system.

Preliminary results show that the addition of a heme dopant reduces repulsive forces when multiple H_2 molecules are placed in a fullerene. Therefore, a second H_2 molecule can be added to C_{60} with a heme dopant with an energy input of 13.1 kJ/mol compared to 20.1 kJ/mol for undoped C_{60}. This increased favourability is likely to occur because the heme group causes a change in the orientation of the H_2 molecules from parallel in undoped C_{60} to perpendicular in heme-doped C_{60} (fig. 18). This is also observed when two or five H_2 molecules were put in C_{60} with a substitutional Pt dopant with a corresponding increase in the favourability of the fullerene–H_2 interactions (section 3.1.5).

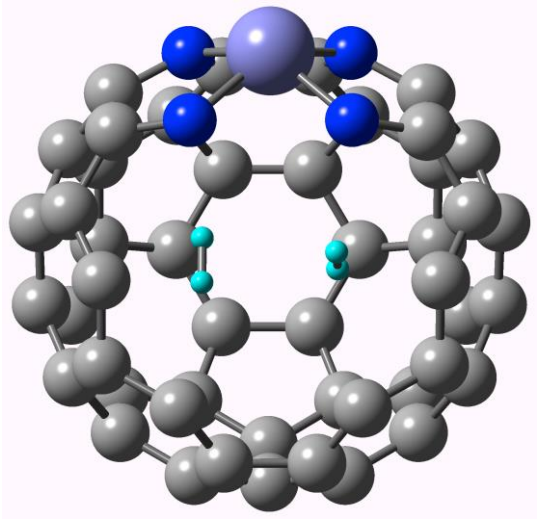

Figure 18 – C_{60} fullerene containing a heme dopant optimized with two internal H_2 molecules showing the perpendicular orientation of the H_2 molecules. The topmost six carbon atoms have been excluded to observe the H_2 molecules more clearly. C = grey, H = light blue, N = dark blue, Fe = purple. Calculated with the B97D functional and 6-311G(d,p) (for C, H, N) and LANL2DZ (for Fe).

A natural bond orbital analysis showed that changes in electron density are similar in C_{60} containing a heme dopant or substitutional platinum. However, the change in electron density of the Fe orbitals are an order of magnitude larger than the Pt orbitals.

4. Conclusions

The present study investigated hydrogen adsorption in curved carbon nanomaterials. Favourable H_2 storage can be achieved when the H_2 molecule is located such that physisorption interactions with many carbon atoms are possible. This requires the $C_{fullerene}$–H_2 distance to be similar to the combined van der Waals radii of carbon and hydrogen, 2.9 Å. Hydrogen storage becomes unfavourable when the $C_{fullerene}$–H_2 or H_2–H_2 distances decrease below 2.9 Å and 2.4 Å (the combined van der Waals radii of the atoms concerned) respectively. Despite these minimum distance requirements, increased confinement (for fullerenes larger than C_{20}) is advantageous because it allows for a higher number of $C_{fullerene}$–H_2 interactions.

Investigation of metal dopants found that platinum affects the electron density of the fullerene during $C_{fullerene}$–H_2 interactions and also influence the H_2 orientation within the fullerene.

These changes can increase the favourability of the $C_{fullerene}$–H_2 interaction but only an occasional weak increase in favourability is observed.

$C_{fullerene}$–H_2 physisorption interactions are typically stronger inside fullerenes because of the concave carbon surface. However, significant $C_{fullerene}$–H_2 physisorption interactions are also observed when H_2 is placed external to C_{20} fullerenes.

It is proposed that a carbon nanotube/fullerene hybride or a C_{20} crystal structure have potential for H_2 storage on board vehicles. In addition, $C_{fullerene}$–H_2 interactions can be strengthened by adding heterogenous dopants, such as a heme group, to the fullerene. Expanded work on H_2 storage in non-carbon fullerenes is currently underway.

Acknowledgements

The authors thank the Centre for Computational Chemistry at the University of Bristol, especially Chris Tothill, for instruction, computational resources, and support during this project. In addition, the authors acknowledge the Natural Sciences and Engineering Research Council of Canada (NSERC) Discovery Grant.

References

1. Barbir, F. (2005) *PEM Fuel Cells: Theory and Practice*. Academic Press
2. Satyapal S., et al. (2007) The U.S. Department of energy's national hydrogen storage project: progress towards meeting hydrogen-powered vehicle requirements. Catalysis Today. 120: 246
3. Lu, Z-H, et al. (2014) Nanocatalysts for Hydrogen Generation from Ammonia Borane and Hydrazine Borane. Journal of Nanomaterials. 2014: 729029
4. Durbin, D. J.; Malardier-Jugroot, C. (2013) Review of hydrogen storage techniques for on board vehicle applications. International Journal of Hydrogen Energy. 38: 14595
5. Jordá-Beneyto, M., et al. (2007) Hydrogen storage on chemically activated carbons and carbon nanomaterials at high pressures. Carbon. 45: 293

6. Yürüm, Y., et al. (2009) Storage of hydrogen in nanostructured carbon materials. International Journal of Hydrogen Energy. 34: 3784

7. Xu, W. C., et al. (2007) Investigation of hydrogen storage capacity of various carbon materials. International Journal of Hydrogen Energy. 32: 2504

8. Tibbetts, G. G., et al. (2001) Hydrogen storage capacity of carbon nanotubes, filaments, and vapor-grown fibers. Carbon. 39: 2291

9. Pupysheva, O. V., et al. (2008) Fullerene Nanocage Capacity for Hydrogen Storage. Nano Letters. 8: 767

10. Elias, D. C., et al. (2009) Control of Graphene's Properties by Reversible Hydrogenation: Evidence for Graphane. Science. 323: 610

11. Sofo, J. O., et al. (2007) Graphane: A two-dimensional hydrocarbon. Physical Review B. 75: 153401

12. Tozzini, V.; Pellegrini, V. (2011) Reversible hydrogen storage by controlled buckling of graphene layers. Journal of Physical Chemistry C. 115: 25523

13. Tozzini, V.; Pellegrini, V. (2013) Prospects for hydrogen storage in graphene. Physical Chemistry Chemical Physics. 15: 80

14. McKean, D. C. (1978) Individual CH bond strengths in simple organic compounds: effects of conformation and substitution. Chemical Society Reviews. 7: 399-422

15. Nijkamp, M. G., et al. (2001) Hydrogen storage using physisorption – materials demands. Applied Physics A. 72: 619

16. Rzepka, M., et al. (1998) Physisorption of Hydrogen on Microporous Carbon and Carbon Nanotubes. Physical Chemistry B. 102: 10894

17. Patchkovskii, S., et al. (2005) Graphene nanostructures as tunable storage media for molecular hydrogen. Proceedings of the National Academy of Sciences. 102: 10439

18. Wang, L.; Yang, R. T. (2008) Hydrogen storage properties of carbons doped with ruthenium, platinum, and nickel nanoparticles. Journal of Physical Chemistry C. 112: 12486

19. Parambhath, V. B., et al. (2011) Investigation of spillover mechanism in palladium decorated hydrogen exfoliated functionalized graphene. Journal of Physical Chemistry C. 115: 15679

20. López-Corral, I., et al. (2011) DFT study of hydrogen adsorption on palladium decorated graphene. Journal of Physical Chemistry C. 115: 4315

21. Rzepka, M., et al. (1998) Physisorption of hydrogen on microporous carbon and carbon nanotubes. Journal of Physical Chemistry B. 102: 10894

22. Wang, Q.; Johnson, J. K. (1999) Molecular simulation of hydrogen adsorption in single-walled carbon nanotubes and idealized carbon slit pores. Journal of Chemical Physics. 110: 577

23. Züttel, A., et al. (2002) Hydrogen storage in carbon nanostructures. International Journal of Hydrogen Energy. 27: 203

24. Meregalli, V.; Parrinello, M. (2001) Review of theoretical calculations of hydrogen storage in carbon-based materials. Applied Physics A. 72: 143

25. Okamoto, Y.; Miyamoto, Y. (2001) Ab initio investigation of physisorption of molecular hydrogen on planar and curved graphenes. Journal of Physical Chemistry B. 105: 3470

26. Scanlon, L. G., et al. (2009) Hydrogen storage based on physisorption. Journal of Physical Chemistry B. 113: 4708

27. Chandrakumar, K. R. S., et al. (2008) Nanoscale curvature-induced hydrogen adsorption in alkali metal doped carbon nanomaterials. Journal of Physical Chemistry C. 112: 15670

28. Henwood, D.; David Carey, J. (2007) *Ab initio* investigation of molecular hydrogen physisorption on graphene and carbon nanotubes. Physical Review B. 75: 245413

29. Oudenhuijzen, M. K., et al. (2001) The Nature of the Pt−H Bonding for Strongly and Weakly Bonded Hydrogen on Platinum. A XAFS Spectroscopy Study of the Pt−H Antibonding Shaperesonance and Pt−H EXAFS. Journal of Physical Chemistry B. 105: 4616

30. Lueking, A. D.; Yang, R. T. (2004) Hydrogen spillover to enhance hydrogen storage—study of the effect of carbon physicochemical properties. Applied Catalysis A: General. 265: 259

31. Li, Y., et al. (2007) Hydrogen Storage on Carbon Doped with Platinum Nanoparticles Using Plasma Reduction. Industrial & Engineering Chemistry Research. 46: 8277

32. Sermon, P. A.; Bond, G. C. (1974) Hydrogen Spillover. Catalysis Reviews: Science and Engineering. 8: 211

33. Wu, G., et al. (2005) Remarkable support effect of SWNTs in Pt catalyst for methanol electrooxidation. Electrochemistry Communications. 7: 1237

34. Bowen, I. S. (1927) Series Spectra of Boron, Carbon, Nitrogen, Oxygen, and Fluorine. Physical Review. 29: 231

35. Yuan, C., et al. (2012) Shell-model study of boron, carbon, nitrogen, and oxygen isotopes with a monopole-based universal interaction. Physical Review C. 85: 064324

36. Choi, C. H., et al. (2012) Binary and Ternary Doping of Nitrogen, Boron, and Phosphorus into Carbon for Enhancing Electrochemical Oxygen Reduction Activity. ACS Nano. 6: 7084

37. Ma, J., et al. (2015) Electronic interaction between platinum nanoparticles and nitrogen-doped reduced graphene oxide: effect on the oxygen reduction reaction. Journal of Materials Chemistry A. 3, 11891

38. Maldonado, S.; Stevenson, K. J. (2005) Influence of Nitrogen Doping on Oxygen Reduction Electrocatalysis at Carbon Nanofiber Electrodes. Journal of Physical Chemistry B. 109: 4707

39. Yang, L., et al. (2011) Boron-Doped Carbon Nanotubes as Metal-Free Electrocatalysts for the Oxygen Reduction Reaction. Angewandte Chemie. 50: 7132

40. Wu. G., et al. (2005) Remarkable support effect of SWNTs in Pt catalyst for methanol electrooxidation. Electrochemistry Communications. 7: 1237

41. Li, Y-H., et al. (2009) A first-principles study of nitrogen- and boron-assisted platinum adsorption on carbon nanotubes. Carbon. 47: 850

42. Durbin, D. J.; Malardier-Jugroot, C. (2010) Density functional theory analysis of metal/graphene systems as a filter membrane to prevent CO poisoning in hydrogen fuel cells. Journal of Physical Chemistry C. 115: 808

43. Durbin, D. J.; Malardier-Jugroot, C. (2012) Theoretical investigation of the use of doped graphene as a membrane support for effective CO removal in hydrogen fuel cells. Molecular Simulation. 38: 1061

44. Frisch, M., et al. (2009) *Gaussian 09*. Vol. Revision A.1. Gaussian Inc.: Wallingford, CT.

45. Lee, C., et al. (1988) Development of the Colle-Salvetti correlation-energy formula into a functional of the electron density. Physical Review B. 37: 785

46. Chen, Z.; Yang, J. (2006) The B3LYP hybrid density functional study on solids. Frontiers of Physics in China. 1: 339

47. Grimme, S., et al. (2010) A consistent and accurate ab initio parametrization of density functional dispersion correction (DFT-D) for the 94 elements H-Pu. Journal of Chemical Physics. 132: 154104

48. Grimme, S., et al. (2011) Effect of the damping function in dispersion corrected density functional theory. Journal of Computational Chemistry. 32: 1456

49. Hay, P. J.; Wadt, W. R. (1985) Ab initio effective core potentials for molecular calculations. Potentials for the transition metal atoms Sc to Hg. Journal of Chemical Physics. 82: 270

50. Wadt, W. R.; Hay, P. J. (1985) Ab initio effective core potentials for molecular calculations. Potentials for main group elements Na to Bi. Journal of Chemical Physics. 82: 284

51. Hay, P. J.; Wadt, W. R. (1985) Ab initio effective core potentials for molecular calculations. Potentials for K to Au including the outermost core orbitals. Journal of Chemical Physics. 82: 299

52. Hehre, W. J., et al. (1969) Self-consistent molecular-orbital methods. I. Use of Gaussian expansions of Slater-type atomic orbitals. Journal of Chemical Physics. 51: 2657

53. Collins, J. B., et al. (1976) Self-consistent molecular orbital methods. XVII. Geometries and binding energies of second-row molecules. A comparison of three basis sets. Journal of Chemical Physics. 64: 5142

54. Grimme, S. (2006) Semiempirical GGA-type density functional constructed with a long-range dispersion correction. Journal of Computational Chemistry. 27: 1787

55. Beheshtian, J., et al. (2012) Theoretical study of CO adsorption on the surface of BN, AlN, BP and AlP nanotubes. Surface Science. 606: 981

56. Dunning Jr., T. H.; Hay, P. J. (1976) *Modern theoretical chemistry*. Vol. 3. Plenum Press: New York

57. Krishnan, R., et al. (1980) Self-consistent molecular orbital methods. XX. A basis set for correlated wave functions. Journal of Chemical Physics. 72: 650

58. *Computational Chemistry List, Ltd.* on-line fullerene database compiled by Cramer at the University of Minnesota

59. TubeGen On-line (version 3.4) created by Frey and Doren at the University of Delaware.

60. Liu, B.; McLean, A. D. (1973) Accurate calculation of the attractive interaction of two ground state helium atoms. Journal of Chemical Physics. 59: 4557

61. Boys, S. F.; Bernardi, F. D. (1970) The calculation of small molecular interactions by the differences of separate total energies. Some procedures with reduced errors. Molecular Physics. 19: 553

62. Simon, S., et al. (1996) How does basis set superposition error change the potential surfaces for hydrogen bonded dimers? Journal of Chemical Physics. 105: 11024

63. Gutowski, M.; Chałasiński, G. (1993) Critical evaluation of some computational approaches to the problem of basis set superposition error. Journal of Chemical Physics. 98: 5540

64. Bakowies, D.; Thiel, W. (1991) MNDO study of large carbon clusters. Journal of the American Chemical Society. 113: 3704

65. Rowland, R. S.; Taylor, R. (1996) Intermolecular Nonbonded Contact Distances in Organic Crystal Structures: Comparison with Distances Expected from van der Waals Radii. Journal of Physical Chemistry. 100: 7384

66. Cabria, I., et al. (2007) The optimum average nanopore size for hydrogen storage in carbon nanoporous materials. Carbon. 45: 2649

67. Weinberg, W. H., et al. (1977) Interaction of H2 and O2 to platinum (111). Journal of Vacuum Science & Technology. 14: 444

68. Groves, M. N., et al. (2012) Improving Platinum Catalyst Durability with a Doped Graphene Support. Journal of Physical Chemistry C. 116: 10548

69. Visscher, L., et al. (1993) The electronic structure of the PtH molecule: Fully relativistic configuration interaction calculations of the ground and excited states. Journal of Chemical Physics. 99: 6704

70. Nasibulin, A. G. (2007) A novel hybrid carbon material. Nature Nanotechnology. 2: 156

71. David, W. I. F., et al. (1991) Crystal structure and bonding of ordered C_{60}. Nature. 353: 147

72. Quo, Y., et al. (1991) Prediction of fullerene packing in C_{60} and C_{70} crystals. Nature. 351: 464